https://doi.org/10.5194/egusphere-2024-4053
Preprint. Discussion started: 10 March 2025

Automated urban flood level detection based on flooded bus dataset using YOLOv8

Yanbin Qiu[a], Xudong Zhou[b],Jiaquan Wan[a,*], Tao Yang[a,c], Lvfei Zhang[a], Yuanzhuo Zhong[a], Leqi Shen[a], Xinwu Ji[a]

[a] College of Hydrology and Water Resources, Hohai University, Nanjing 210024, China

[b] Institute of Hydraulics and Ocean Engineering, Ningbo University, Ningbo 315000, China

[c] Institute of Water Resources and Technology, Hohai University, Nanjing 210024, China

Corresponding Author:

Jiaquan Wan

College of Hydrology and Water Resources, Hohai University, Nanjing 210024, China

Email: 775290095@qq.com

ABSTRACT

Rapid and accurate acquisition of urban flood information is crucial for flood prevention, disaster mitigation, and emergency management. With the development of mobile internet, crowdsourced images on social media have been emerged as a novel and effective data source for flood information collection. However, selecting appropriate targets and employing suitable methods to determine flooding level has not been well investigated. This study proposes a method to assess urban flood risk levels based on the submerged status of buses captured in social media images. First, a dataset containing 1008 images in complex scenes is constructed from social media. The images are annotated using Labelimg, and expanded with a data augmentation strategy. Four YOLOv8 configurations are validated for their ability to identify urban flood risk levels. The validation process involves training the models on original datasets, augmented datasets, and datasets representing complex scenes. Results demonstrate that, compared to traditional reference objects (e.g., cars), buses exhibit greater stability and higher accuracy in identification of urban flood risk levels due to their standardized height and widespread presence as they remain service during flood events. The data augmentation strategy enhances the model's mAP50 and mAP50-95 metrics by over 10% and 20%, respectively. Additionally, through comparative analysis of YOLOv8 configurations, YOLOv8s demonstrates superior results and achieves an effective balance between accuracy, training time, and computational resources, recommended for the identification of urban flood risk levels. This method provides a reliable technical foundation for real-time flood risk assessment and emergency management of urban transportation systems, with substantial potential for practical applications.

Keyword: Urban Flooding; Automatic Detection; Computer Vision; Object Detection

https://doi.org/10.5194/egusphere-2024-4053
Preprint. Discussion started: 10 March 2025

1. Introduction

With the intensification of global climate change, extreme precipitation events have increasingly triggered urban pluvial flooding, severely disrupting the operation of major cities (Guan et al., 2015). Concurrently, the proportion of impervious surfaces has been rising due to rapid urbanization, significantly diminishing the infiltration capacity of urban landscapes and resulting in an increase in surface runoff (Chaudhary et al., 2020). This has led to more frequent urban flooding incidents, imposing substantial impacts and losses on urban infrastructure, transportation networks, and human wellbeing. For instance, on July 20, 2021, a rare extreme rainfall event, with a record-breaking maximum hourly rainfall of 201.9 mm, driven by Typhoon In-Fa struck Zhengzhou, Henan Province, China, leading to severe urban inundation that resulted in 292 casualties and direct economic losses reaching 53.2 billion (Yang and Wang, 2022).

In the event of urban flooding, the ability to rapidly and accurately identify flood risk levels is crucial for urban flood prevention, mitigation, and emergency response decision making (Fohringer et al., 2015; Qian et al., 2022; Smith et al., 2017). Currently, urban waterlogging monitoring primarily relies on water level gauges (Fohringer et al., 2015). Although water level gauges can monitor flood depth in real-time, their deployment and maintenance are costly, and the monitoring range is restricted by the installation locations, limiting their suitability for wider spatial coverage (Chaudhary et al., 2020; Fohringer et al., 2015; Paul et al., 2020). Microwave remote sensing methods have limitations in spatial-temporal resolution and data frequency, and are susceptible to interference from clouds and obstructions, rendering them unable to determine flood depth (Chaudhary et al., 2020; DeVries, 2020; Liang, 2020). An intelligent and low-cost technology capable of identifying urban flood risks with extensive spatial coverage is urgently needed.

In recent years, with the rapid development of social media and mobile internet, the application of social media data in flood monitoring and risk assessment has garnered extensive attention (Baranowski et al., 2020; Kankanamge et al., 2020; Li et al., 2023; Rosser et al., 2017; Smith et al., 2017). Platforms like Weibo, Twitter and Douyin provide users with channels to share flood information in real time, where user-generated content (UGC) contains rich flood imagery and geolocation data, offering a novel data source for urban flood level detection research (Iqbal et al., 2021). Concurrently, significant advancements have been made in computer vision technology, particularly in the application of convolutional neural networks (Voulodimos et al., 2018) , opening new avenues for the analysis of vast amounts of flood imagery data. Current studies have attempted to use objects in social media images, such as bridges (Bhola et al., 2018), roadside barriers

https://doi.org/10.5194/egusphere-2024-4053
Preprint. Discussion started: 10 March 2025

(Jiang et al., 2019), bicycles (Chaudhary et al., 2020), traffic cones (Jiang et al., 2020), traffic signs (Alizadeh Kharazi and Behzadan, 2021), water level markers (Jafari et al., 2021), and pedestrians (Li et al., 2023), as reference points for flood level estimation. While specific reference objects have shown promising results in studies, their infrequent occurrence hinders their broad application in urban settings. Pedestrians are prevalent in urban areas, but their low image resolution and diminished presence in severely flooded zones reduce their reliability and practicality as reference points for water level estimation.

Vehicles serve as ideal reference objects for recognizing urban flood levels, attributed to their stable morphological features, widespread availability, and ease of detection. Current research leverages vehicles for urban flood water level identification. For example, Park et al. used Mask R-CNN to detect the submerged state of vehicles or their wheels as an indicator of flood levels. (Huang et al., 2020; Park et al., 2021), while Wan et al. utilized the YOLO series models for urban flood risk assessment and detection (Puliti and Astrup, 2022; Redmon et al., 2016; Wan et al., 2024; Zhong et al., 2024). However, most studies use cars as reference objects; yet, the diversity of car types (e.g., sedans, SUVs, and pickup trucks) introduces significant variations in height and dimensions, affecting model generalization. Furthermore, the limited height of car bodies means they cannot provide effective water level information once submerged up to the roof, and their lower frequency of appearance in extreme weather makes it challenging to collect image datasets.

In comparison, buses, as a critical component of urban transportation systems, possess standardized heights and structures with minimal variation between models, making them a more ideal reference object for flood water level monitoring. Buses overcome the limitations posed by cars, such as variations in size and limited height. Additionally, buses primarily operate in busy or essential areas, and their ability to withstand submersion is crucial for the continued operation of the urban public transportation system. Flood level recognition based on the submerged status of buses can intelligently assess their water-related risks, providing valuable support for urban transportation emergency management.

In response to the gaps in existing research, this study aims to create a comprehensive dataset of submerged buses by sourcing flood images from social media platforms. Based on urban flood safety standards and bus height characteristics, the submerged states of buses will be categorized into specific levels. The dataset includes complex scenes (e.g., nighttime, occlusions, and incomplete bus bodies) to enhance data diversity. The YOLOv8 algorithm, as the most recent iteration of the YOLO series, has exhibited outstanding accuracy and rapid detection performance on the standard COCO (Common Objects in Context)

https://doi.org/10.5194/egusphere-2024-4053
Preprint. Discussion started: 10 March 2025

dataset. In this study, the YOLOv8 model is trained on a purpose-built dataset to improve its performance in identifying urban flood water levels with precision. This study introduces an innovative approach to flood level detection by leveraging the submerged states of buses, addressing the limitations of traditional recognition methods based on cars and other reference objects and overcoming the limitations of conventional monitoring techniques in broader applications. Specifically, the objectives of this study include:

1) Developing a comprehensive dataset of submerged buses to examine the relationship between bus submersion and flood water levels.
2) Evaluating the performance of YOLOv8 configurations in assessing flood severity through original and augmented data training, as well as experiments involving complex scenes.
3) Proposing configuration recommendations for YOLOv8 aims to address diverse application scenarios, ensuring efficient deployment in varied urban environments.

This paper is structured as follows: Section 2 provides a detailed description of the dataset construction, data augmentation strategies, and YOLOv8 model configurations, explains the experimental design, model evaluation metrics. Section 3 explains experimental results, followed by a comparative analysis of the findings. Section 4 discusses the experimental results and offers configuration recommendations for YOLOv8. Finally, Section 5 provides a summary of the main conclusions and highlights potential directions for future research.

2. Methodology

2.1 Data acquisition and processing

2.1.1 Data acquisition

In this study, a comprehensive dataset of submerged buses was constructed, comprising 1,008 images that capture buses in various statues of submersion. These submerged bus images were collected through keyword searches such as urban flooding and submerged bus on Baidu and Google, screenshots of relevant frames in short videos on Douyin, browsing urban flood news, and obtaining images from WeChat public accounts. Due to the diverse sources of image data, the images in exhibit differences in resolution and size. When selecting bus images, this study included complex and challenging scenes, such as nighttime scenes, partial occlusions, and incomplete buses, to ensure the dataset's diversity. The inclusion of these scenes may help enhance the diversity of the dataset, potentially enabling the trained model to better handle various flood scenes.

https://doi.org/10.5194/egusphere-2024-4053
Preprint. Discussion started: 10 March 2025

2.1.2 Data annotation

This study assesses flood risk levels based on the submersion status of buses. To ensure accurate detection of the entire bus, four flood levels were defined, with detailed information on each flood level and corresponding bus examples provided in Table 1. Using Labelimg, a widely used annotation tool for object detection model training, the 1,008 acquired images were annotated to identify 1,562 instances, which were stored in YOLO format for subsequent training. Based on different states of bus movement, annotation types were divided into two categories: holistic and segmented. In holistic annotation, the entire bus is assigned a single flood level, while in segmented annotation, specific parts of the bus correspond to different levels, as illustrated in Fig. 1.

Table 1
Flooded bus dataset: bus instances and flood levels.

Flood levels	Analysis of bus submersion depths	Range of water depth	Number of instances
Level1	bottom of wheels submerged; inner wheel contour not visible	0~20 cm	296
Level2	between bottom of wheels and halfway up the tires, between bottom of wheels and top edge of license plate, water reaches 1/4 of the step at bottom of door	20~45 cm	585
Level3	between halfway up the tires and full tire coverage, between top edge of license plate and bottom edge of windshield	45~100 cm	371
Level4	above the bottom edge of the windshield, fully submerged tires	>100 cm	310

https://doi.org/10.5194/egusphere-2024-4053
Preprint. Discussion started: 10 March 2025

Fig. 1. Examples of dataset annotations: (a) The entire bus is assigned a single flood level; (b) The specific part of bus is assigned different levels.

2.1.3 Data augmentation

The original dataset, comprising 1,008 images, is relatively small in scale, necessitating its enhancement and expansion to increase background complexity, prevent overfitting, and improve robustness. Image data augmentation methods can be broadly categorized into two types: luminosity distortions and geometric distortions(Li et al., 2023). The former involves adjusting image brightness, contrast, hue, saturation, and adding noise, while the latter encompasses random scaling, cropping, flipping, and rotation operations. In this study, horizontal and vertical flipping, rotation, and random cropping were applied to augment the original dataset, as illustrated in Fig. 2. All images in the augmented dataset were annotated using Labelimg and stored in YOLO format. Additionally, considering the potential for manual annotation bias, a review process was conducted to verify the correctness of all bounding boxes and annotations related to flood risk levels.

https://doi.org/10.5194/egusphere-2024-4053
Preprint. Discussion started: 10 March 2025

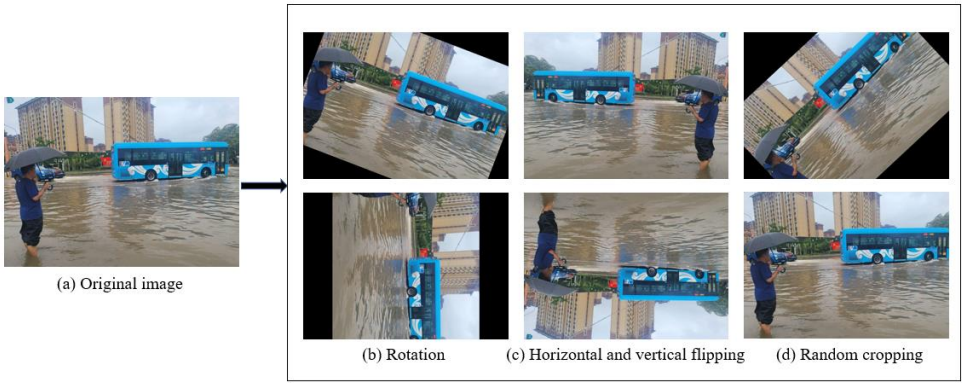

Fig. 2. Examples of dataset augmentations: (a) Original image; (b) Rotation; (c) Horizontal and vertical flipping; (d) Random cropping.

2.2 Object detection model

A key feature of the YOLO model is its ability to achieve an optimal trade-off between speed and accuracy, enabling rapid and precise object detection across a wide range of application scenes (Wan et al., 2024). This study constructed an object detection model based on the YOLOv8 source code, which operates on convolutional neural networks (CNN). YOLOv8 is an integrative and enhanced version building on previous YOLO generations and represents the latest iteration in the YOLO series. This version significantly improves computational efficiency and inference speed by optimizing the network architecture and refining inference algorithms. Moreover, YOLOv8 demonstrates higher stability in multi-object detection tasks under complex scenes, particularly with its advanced features such as automated hyperparameter tuning and dynamic convolution modules. These enhancements further boost the model's flexibility and adaptability, making it more capable of meeting the diverse requirements of real-world applications.

The YOLOv8 processing workflow includes image preprocessing, multi-level feature extraction through CNN, and multi-scale feature fusion via a feature pyramid and path aggregation network. Following this, adaptive anchor boxes are used for bounding box regression and classification prediction, with non-maximum suppression applied to eliminate redundant bounding boxes. The model ultimately outputs the target's class, bounding box, and confidence score, ensuring a balance between detection accuracy and efficiency.

As shown in Fig. 3, the YOLOv8 network architecture is composed of three primary parts: Backbone, Neck, and Head. The Backbone consists of five convolutional modules, four C2f modules, and a SPPF module, all designed for feature extraction. The Neck refines and integrates features derived from the

https://doi.org/10.5194/egusphere-2024-4053
Preprint. Discussion started: 10 March 2025

Backbone, improving both the precision and reliability of object detection. The Head utilizes a decoupled structure to handle feature maps across multiple scales, generating the final detection outputs.

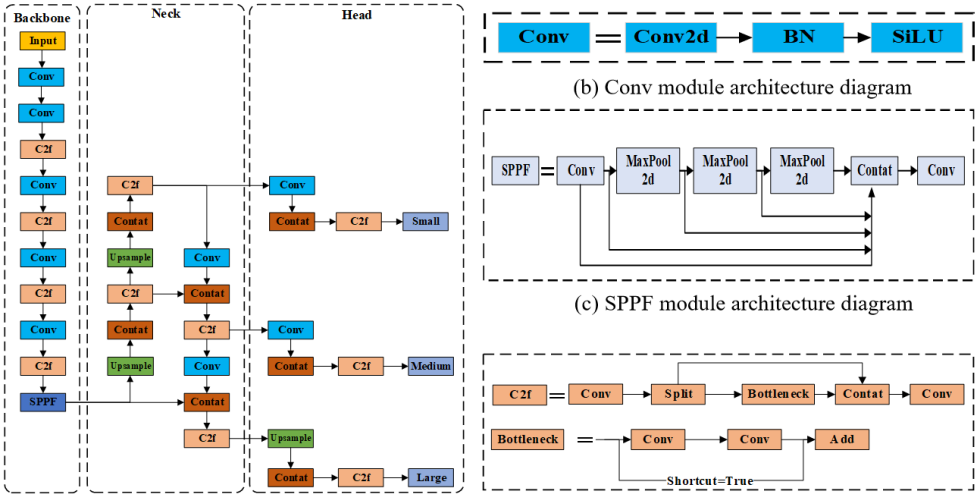

(a) YOLOv8 network diagram (b) Conv module architecture diagram (c) SPPF module architecture diagram (d) C2f module architecture diagram

Fig. 3. The YOLOv8 network structure: (a) YOLOv8 network diagram; (b) Conv module architecture diagram; (c) SPPF module architecture diagram; (d) C2f module architecture diagram.

2.2.1 Experiment on object detection model

Following data augmentation, the original dataset was expanded to 2,184 images for model training. In this study, four different YOLOv8 configurations—YOLOv8n, YOLOv8s, YOLOv8m, and YOLOv8l—were used for training, each designed with specific network depths and widths to address varying application requirements. Table 2 presents the key characteristics of these four YOLOv8 configurations. The number of layers reflects the depth of the model, with a greater number of layers indicating a deeper model capable of capturing higher-level semantic features. However, this also leads to increased computational complexity. Parameters refer to the total number of learnable weights and biases within the model. A higher number of parameters signifies stronger representational capacity, making the model suitable for more complex tasks, but it also requires greater computational resources and longer training times.

Table 2
The primary characteristics of the four YOLOv8 configurations.

Model	Size	Layers	Params (M)	mAP50-95on val (%)	FLOPs (B)	Speed CPU ONNX (ms)	Speed A100 TensorRT (ms)
YOLOv8n	640	225	3.2	37.3	8.7	80.4	0.99
YOLOv8s	640	225	11.2	44.9	28.6	128.4	1.20
YOLOv8m	640	295	25.9	50.2	78.9	234.7	1.83
YOLOv8l	640	365	43.7	52.9	165.2	375.2	2.39

2.2.2 Experimental setup

https://doi.org/10.5194/egusphere-2024-4053
Preprint. Discussion started: 10 March 2025

The model was implemented using PyTorch, a framework offering libraries for object detection models. Training was performed on NVIDIA Quadro RTX 3090 GPU. The original dataset contained 1,008 images, with 90% allocated for training and the remaining 10% for validation. The initial input size was set to 640 × 640, with a batch size of 16 and 100 training epochs. In the data augmentation experiment, the augmented dataset expanded to 2,184 images, with 90% for training and 10% for validation, while all other settings remained the same as previously described.

2.2.3 Complex scenes prediction experiment

The performance of object detection models on the validation dataset does not fully represent its overall capabilities, as view of the bus, impacted by camera angle and distance, introduces numerous sources of interference. To address this, a complex scene prediction experiment was designed in this study to assess the detection capabilities of the different YOLOv8 configurations under challenging urban flood environments.

In this experiment, YOLOv8 models trained on either the original or augmented datasets were used to conduct complex scene predictions, evaluating their performance under challenging conditions. Fig. 4 presents two particularly demanding scene, not in the existing dataset, Fig. 4a shows a rainy scene with multiple vehicles, where the incomplete view of the bus, impacted by camera angle and distance, introduces numerous sources of interference, increasing detection complexity. Fig. 4b depicts a nighttime scene of a submerged bus, where low light and poor image quality significantly elevate the difficulty of detection.

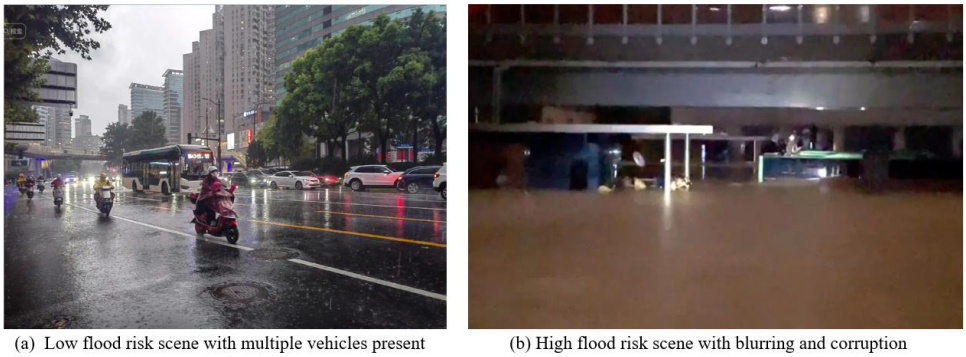

(a) Low flood risk scene with multiple vehicles present (b) High flood risk scene with blurring and corruption

Fig. 4. Two complex urban flooding scenes: (a) Low flood risk scene with multiple vehicles present; (b) High flood risk scene with blurring and corruption.

2.2.4 Comparative experiment with YOLOv5 model

Although the introduction mentions that YOLOv8 is the latest algorithm in the YOLO series, a lack of comparative experimental data would be unconvincing. This study will compare and analyze the configuration demonstrating superior performance in the experiments with the corresponding configuration

https://doi.org/10.5194/egusphere-2024-4053
Preprint. Discussion started: 10 March 2025

in the YOLOv5 model. The experiments include training on the original dataset, training with data augmentation, and complex scene prediction, following the same experimental setup described earlier.

2.3 Model evaluation

The widely recognized evaluation metrics, such as precision (P), recall (R), and F1 scores are as follows:

$$Precision = \frac{TP}{TP + FP} \tag{1}$$

$$Recall = \frac{TP}{TP + FN} \tag{2}$$

$$F1 = \frac{2 \times Precision \times Recall}{Precision + Recall} \tag{3}$$

Precision (P) quantifies the model's false detection rate, while Recall (R) evaluates its true detection rate. The F1-score evaluates model performance, particularly in object detection tasks, as it combines both P and R, representing their harmonic mean, where True Positive (TP) refers to the count of objects correctly identified as positive, True Negative (TN) denotes the count of non-objects accurately classified as negative, False Positive (FP) indicates the count of non-objects incorrectly classified as positive, and False Negative (FN) represents the count of objects wrongly classified as negative.

In this study, mean Average Precision (mAP), a well-established evaluation indicator, is utilized as the primary criterion to evaluate the performance of different YOLOv8 configurations in detecting bus submersion states. The mAP is computed by summing the average precision across all labels and dividing the result by the total number of categories. A higher mAP value signifies improved average accuracy of the model, indicating enhanced overall detection performance. The formula for calculating mAP is as follows:

$$mAP = \frac{1}{n}\sum_{i=1}^{n} AP_i = \frac{1}{n}\sum_{i=1}^{n}\int_0^1 P_i(R_i)dR_i \tag{4}$$

As the output quality of the model varies with changes in the Intersection over Union (IoU) threshold, it is standard practice to evaluate model performance across multiple IoU thresholds. IoU quantifies the overlap between the detection box (generated by the algorithm) and the ground truth box (annotated using labeling software), with a range of values from 0 to 1. A higher IoU value signifies better prediction accuracy, representing a greater overlap between the detection box and the ground truth box. The formula for calculating IoU is as follows:

https://doi.org/10.5194/egusphere-2024-4053
Preprint. Discussion started: 10 March 2025

$$IoU = \frac{A \cap B}{A \cup B} \quad (5)$$

where A denotes the area of the detection box, while B refers to the area of the ground truth box.

mAP50 and mAP50-95 are core metrics for evaluating object detection model performance, each measuring the model's average detection precision under different IoU threshold conditions. mAP50 indicates the average precision computed at an IoU threshold of 0.5, where an overlap of over 50% between the detection box and ground truth box qualifies as a correct detection. This metric primarily reflects the model's basic object detection capability. mAP50-95, on the other hand, is the mean average precision calculated across ten different IoU thresholds, from 0.5 to 0.95 in 0.05 increments. This metric averages AP across multiple IoU thresholds, providing a comprehensive assessment of the model's performance. A higher mAP50-95 value indicates stronger generalization ability across varying degrees of overlap within the same scene. Collectively, mAP50 and mAP50-95 provide a thorough and objective evaluation of model prediction accuracy and are extensively utilized in the domain of object detection.

3. Result

3.1 Training experimental results

3.1.1 Analysis of training results on the original dataset

This subsection provides a comparative evaluation of the training outcomes of the different YOLOv8 models on the original dataset. Each model was trained under the experimental settings outlined in Section 3.1. Fig. 5 illustrates the trend of mAP for each model during the training period, while Fig. 6 presents the prediction performance of each model across individual classes.

As illustrated in Fig. 5a, following 100 epochs of training, the four models (YOLOv8n, YOLOv8s, YOLOv8m, YOLOv8l) each reach convergence, achieving mAP50 values on the validation dataset of 0.618, 0.662, 0.611, and 0.639, respectively. YOLOv8s exhibits superior performance in this object detection task, maintaining a higher mAP50 across the training duration compared to the other configurations. YOLOv8l shows pronounced oscillations during the early training stages, requiring a longer stabilization period. Furthermore, it is observable that mAP50 for all models increases rapidly in the early epochs (0-20), after which the growth rate decelerates and plateaus. Notably, an increase in network width (param) and depth (layer) for YOLOv8 does not yield a substantial improvement in mAP50.

https://doi.org/10.5194/egusphere-2024-4053
Preprint. Discussion started: 10 March 2025

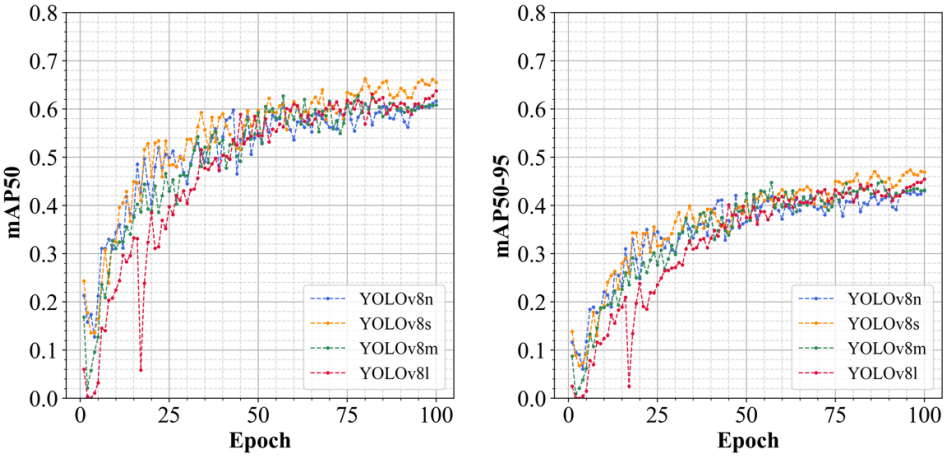

(a) The trend of mAP50 (b) The trend of mAP50-95

Fig. 5. The mAP of the validation dataset throughout the training process (a) The trend of mAP50; (b) The trend of mAP50-95.

As shown in Fig. 6, the detection performance of the four YOLOv8 models varies across different flood risk levels. The YOLOv8s model demonstrates superior average precision across all flood risk categories, with an mAP50 of 0.662. For low flood risk category identification (level 1), all models achieve satisfactory detection results. However, for higher flood risk categories, the detection performance of YOLOv8n, YOLOv8m, and YOLOv8l is below expectations, with only YOLOv8s effectively capturing the submersion characteristics of buses at high water levels, thereby achieving relatively accurate identification. Although the YOLOv8l model has higher complexity and a larger parameter scale, its AP values for the level 3 and level 4 categories are 0.591 and 0.530, respectively, significantly lower than those of the YOLOv8s model, which are 0.632 and 0.602. This suggests that, for detecting high flood risk features, increased model complexity does not inherently result in improved detection accuracy.

https://doi.org/10.5194/egusphere-2024-4053
Preprint. Discussion started: 10 March 2025

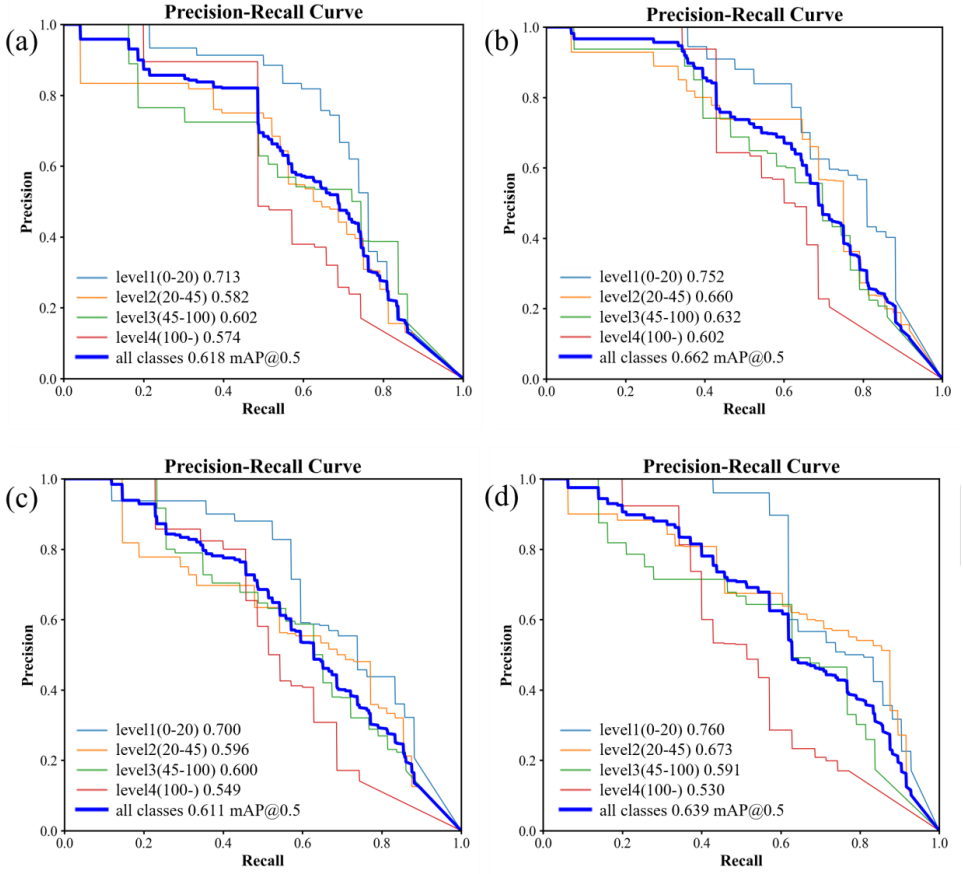

Fig. 6. Precision-recall curve for each class of validation process: (a) YOLOv8n Validation Results; (b) YOLOv8s Validation Results; (c) YOLOv8m Validation Results; (d) YOLOv8l Validation Results.

3.1.2 Analysis of training results on the augmented dataset

This subsection provides a comparative evaluation of the training outcomes of the different YOLOv8 models on the augmented dataset. Fig. 7 illustrates the mAP trend, while Fig. 8 presents the prediction performance of each model.

As depicted in Fig. 7a, after 100 training epochs, the four models (YOLOv8n, YOLOv8s, YOLOv8m, YOLOv8l) each converge, reaching mAP50 values on the validation dataset of 0.722, 0.734, 0.716, and 0.703, respectively. Data augmentation has yielded substantial improvements in both mAP50 and mAP50-95 for all models, which will be analyzed in further detail in the next subsection. Following augmentation, YOLOv8s consistently outperforms the other models, with a higher mAP50 value. After incorporating data augmentation, the initial jump phenomenon observed during YOLOv8l training disappears, resulting in smoother curves and a more stable optimization process. However, compared to other models, the

https://doi.org/10.5194/egusphere-2024-4053
Preprint. Discussion started: 10 March 2025

288 performance improvement of YOLOv8l during the early stages of training remains relatively slower. This
289 may be attributed to the model's higher complexity and larger parameter scale.

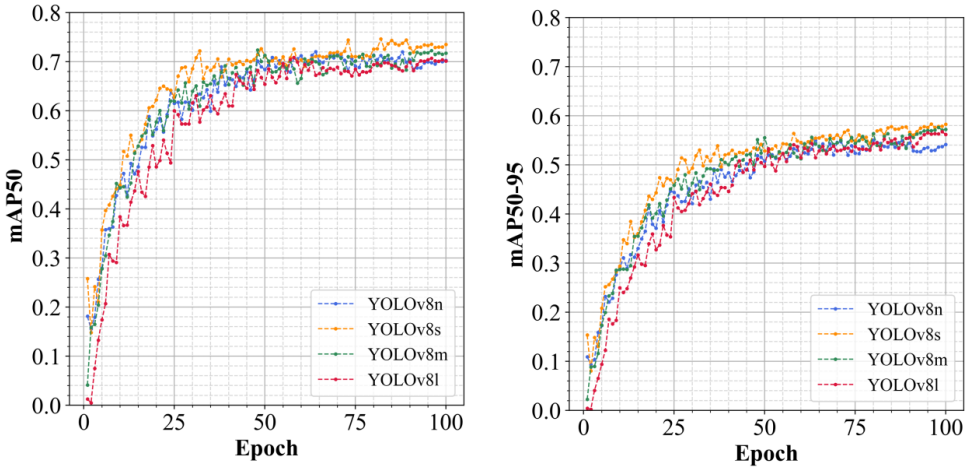

(a) The trend of mAP50 (b) The trend of mAP50-95

290
291 **Fig. 7.** The mAP of the validation dataset throughout the training process after data augmentation: (a) The
292 trend of mAP50; (b) The trend of mAP50-95.

293 As illustrated in Fig. 8, following data augmentation, the four YOLOv8 models exhibit similar
294 performance in detecting each flood risk level. The highest overall effectiveness is found in YOLOv8s,
295 achieving an mAP50 of 0.734, with consistently high precision and recall across all flood risk categories.
296 Post-augmentation, all models effectively capture the submersion characteristics of buses at various water
297 levels, with AP values for each category exceeding 0.67, indicating robust performance on the validation
298 dataset. Moreover, data augmentation significantly improved the detection capabilities of all models for
299 higher-level categories (Level 3 and Level 4), as evidenced by the Precision-Recall curves shifting closer to
300 the upper-right corner. For example, in the YOLOv8n model, the AP value for Level 3 increased from 0.602
301 to 0.712, and for Level 4, from 0.574 to 0.746. Similarly, in the YOLOv8l model, the AP value for Level 3
302 rose from 0.600 to 0.685, and for Level 4, from 0.549 to 0.679. Data augmentation enhanced the diversity
303 of training samples, effectively mitigating the interference caused by variations in viewpoint and object scale.
304 This not only improved the model's ability to detect higher-level targets but also enhanced the overall
305 detection performance.

https://doi.org/10.5194/egusphere-2024-4053
Preprint. Discussion started: 10 March 2025

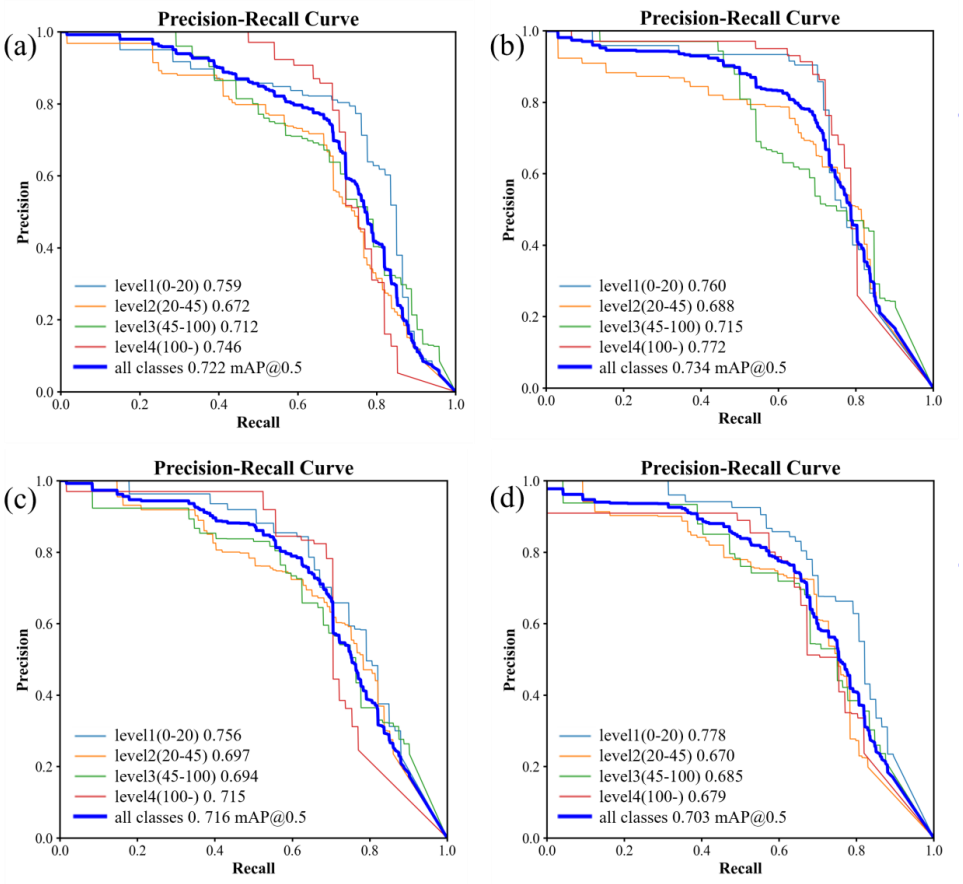

Fig. 8. Precision-recall curve for each class of validation process after data augmentation: (a) YOLOv8n Validation Results; (b) YOLOv8s Validation Results; (c) YOLOv8m Validation Results; (d) YOLOv8l Validation Results.

This study provides a comparative analysis of the detection performance of different YOLOv8 model configurations before and after data augmentation. Table 3 presents the mAP50, mAP50-95, and training times for the optimal YOLOv8 models

Table 3
mAP and training time for four YOLOv8 configurations: pre- and post-data augmentation.

YOLO v8	mAP50 (%)			mAP50-95 (%)			training time (h)	
	original dataset	augmented dataset	increase	original dataset	augmented dataset	increase	original dataset	augmented dataset
n	61.7	72.2	17.0	43.0	55.2	28.4	0.102	0.325
s	66.0	73.4	11.2	47.5	58.2	22.5	0.152	0.483
m	61.2	71.6	17.0	45.0	57.4	27.6	0.293	0.930
l	63.8	70.3	12.2	45.4	56.6	24.7	0.438	1.390

As indicated in Table 3, data augmentation led to significant enhancements in model detection performance, with substantial increases in both mAP50 and mAP50-95 across all configurations. For mAP50, all models demonstrated improvements exceeding 10%, while mAP50-95 gains surpassed 20% for each

https://doi.org/10.5194/egusphere-2024-4053
Preprint. Discussion started: 10 March 2025

configuration. YOLOv8m and YOLOv8n exhibited the highest mAP50 increases, whereas YOLOv8s showed the smallest gain at 11.2%. In terms of mAP50-95, YOLOv8n achieved the greatest improvement, rising from 43.0% to 55.2% (28.4% increase), while YOLOv8s displayed the smallest increase at 22.5%.

In terms of overall performance, YOLOv8s achieved the highest mAP50 and mAP50-95 values across all configurations, reaching 73.4% and 58.2%, respectively, with a moderate training time. By contrast, YOLOv8l achieved similar mAP50 and mAP50-95 values but required nearly triple the training time. Similarly, YOLOv8m showed performance close to that of YOLOv8s, though with a nearly doubled training time.

3.2 Experimental results in complex scenes

3.2.1 Validation results of models on the original dataset

This section presents a comparative evaluation of the validation outcomes for the four optimized YOLOv8 models trained on the original dataset. The numbers on the image represent the confidence level of the model for the detection results. As shown in Fig. 9, all four models can detect the flood risk level of the bus. However, only YOLOv8l correctly identifies it as level 1, albeit with low confidence, while the other models incorrectly classify it as level 2. At low flood risk levels, none of the models effectively capture the critical distinguishing features, highlighting limitations in their generalization capabilities.

https://doi.org/10.5194/egusphere-2024-4053
Preprint. Discussion started: 10 March 2025

(a) Detection outcomes obtained using YOLOv8n (b) Detection outcomes obtained using YOLOv8s

(c) Detection outcomes obtained using YOLOv8m (d) Detection outcomes obtained using YOLOv8l

Fig. 9. Comparison of YOLOv8 detection results in low flood risk scene with multiple vehicles present (pre-augmentation): (a) Detection outcomes obtained using YOLOv8n; (b) Detection outcomes obtained using YOLOv8s; (c) Detection outcomes obtained using YOLOv8m; (d) Detection outcomes obtained using YOLOv8l.

Moreover, Fig. 10 presents the validation results at a high flood risk level. All four optimal YOLOv8 models successfully detect the blurred bus in the image and identify its submerged state with high confidence. For the bus located at the upper-right edge of the image, none of the models detected it due to low lighting, though they were able to make partial level assessments. The models have learned to extract key features associated with incomplete bus bodies from the dataset. Furthermore, YOLOv8l incorrectly classified the bus station and surrounding environment as level 4 submersion.

https://doi.org/10.5194/egusphere-2024-4053
Preprint. Discussion started: 10 March 2025

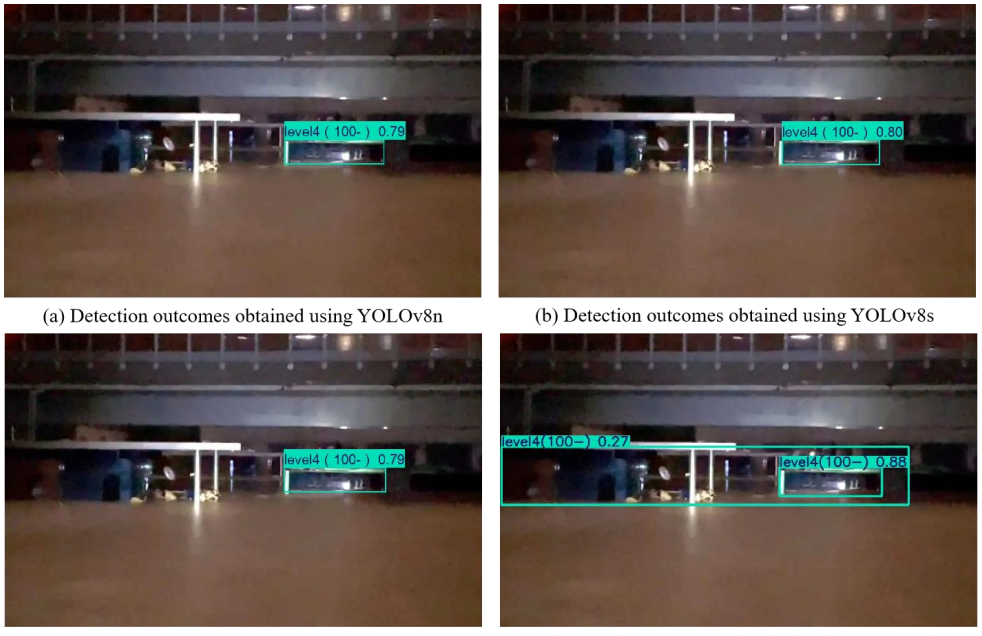

(a) Detection outcomes obtained using YOLOv8n (b) Detection outcomes obtained using YOLOv8s

(c) Detection outcomes obtained using YOLOv8m (d) Detection outcomes obtained using YOLOv8l

Fig. 10. Comparison of YOLOv8 detection results in high flood risk scene with blurring and corruption (pre-augmentation): (a) Detection outcomes obtained using YOLOv8n; (b) Detection outcomes obtained using YOLOv8s; (c) Detection outcomes obtained using YOLOv8m; (d) Detection outcomes obtained using YOLOv8l.

3.2.2 Validation results of models on the augmented dataset

This section provides a comparative evaluation of the validation outcomes for the four optimized YOLOv8 models after data augmentation. As shown in Fig. 11, all four models accurately detect the flood risk level of the bus with high confidence. In this detection, the best performance is found inYOLOv8n, exhibiting higher confidence levels than the other models. Besides, both YOLOv8s and YOLOv8m unexpectedly generated a level 2 prediction box during bus detection.

https://doi.org/10.5194/egusphere-2024-4053
Preprint. Discussion started: 10 March 2025

(a) Detection outcomes obtained using YOLOv8n (b) Detection outcomes obtained using YOLOv8s

(c) Detection outcomes obtained using YOLOv8m (d) Detection outcomes obtained using YOLOv8l

Fig. 11. Comparison of YOLOv8 detection results in low flood risk scene with multiple vehicles present (post-augmentation): (a) Detection outcomes obtained using YOLOv8n; (b) Detection outcomes obtained using YOLOv8s; (c) Detection outcomes obtained using YOLOv8m; (d) Detection outcomes obtained using YOLOv8l.

Fig. 12 presents the validation results at a high flood risk level. All four optimal YOLOv8 models successfully detect the blurred bus in the image, accurately identifying its submerged state with high confidence. The highest confidence is found in YOLOv8s, without any false detections. However, none of the models detected the bus body located at the upper-right edge of the image, even after data augmentation. Besides, YOLOv8m and YOLOv8l incorrectly classified the bus station and background environment as level 4 submersion.

In summary, data augmentation resulted in notable improvements in both recognition accuracy and confidence across the four optimal models, enhancing their ability to accurately detect bus submersion states. In addition, detection performance under low-light conditions remains an area requiring further refinement.

https://doi.org/10.5194/egusphere-2024-4053
Preprint. Discussion started: 10 March 2025

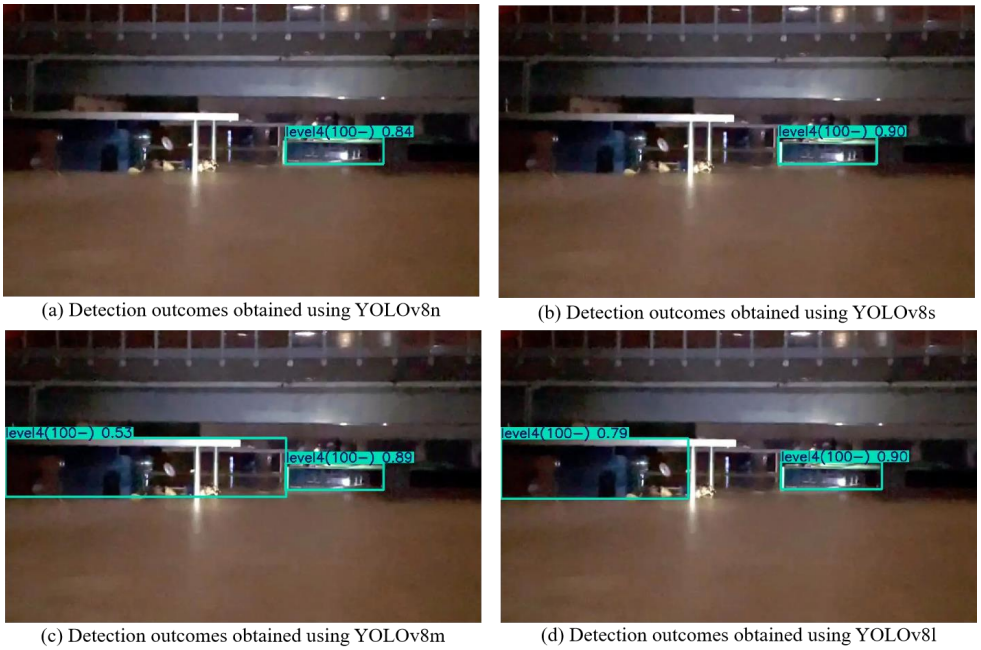

(a) Detection outcomes obtained using YOLOv8n (b) Detection outcomes obtained using YOLOv8s

(c) Detection outcomes obtained using YOLOv8m (d) Detection outcomes obtained using YOLOv8l

Fig. 12. Comparison of YOLOv8 detection results in high flood risk scene with blurring and corruption (pre-augmentation): (a) Detection outcomes obtained using YOLOv8n; (b) Detection outcomes obtained using YOLOv8s; (c) Detection outcomes obtained using YOLOv8m; (d) Detection outcomes obtained using YOLOv8l.

3.3 Experimental results compared with YOLOv5

3.3.1 Analysis of training experiment results

Fig. 13 displays the precision-recall curves from the training results. A comparison reveals that YOLOv8s outperforms YOLOv5s on both the original and augmented datasets, indicating that YOLOv8s achieves higher detection accuracy in image recognition tasks. On the original dataset, YOLOv5s attains an mAP50 of 0.555, while YOLOv8s reaches 0.662, reflecting a performance gap of 19.3%. After data augmentation, although the performance gap between YOLOv5s and YOLOv8s narrows, YOLOv8s continues to lead. Additionally, results from the two training experiments with YOLOv5 indicate that data augmentation has a substantial impact on enhancing the training effectiveness of YOLO models

https://doi.org/10.5194/egusphere-2024-4053
Preprint. Discussion started: 10 March 2025

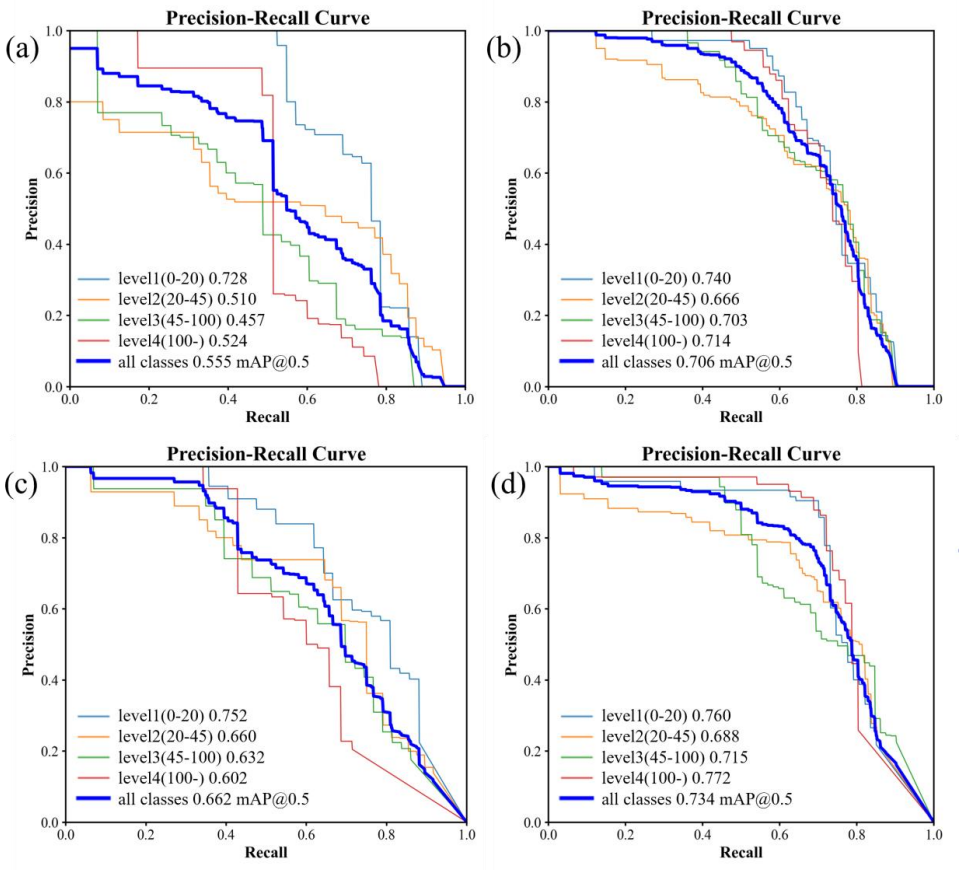

Fig. 13. Precision-recall curves from the training results: (a) YOLOv5s validation results on original dataset; (b) YOLOv5s validation results on augmented dataset; (c) YOLOv8s validation results on original dataset; (d) YOLOv8s validation results on augmented dataset.

3.3.2 Analysis of scene prediction experiment results

This section evaluates the stability and effectiveness of YOLOv5s and YOLOv8s under challenging conditions by testing their performance in two complex urban scenes. Fig. 14 and Fig. 15 illustrate the detection results of YOLOv5s and YOLOv8s in low and high flood risk scenes, respectively. In the low-risk scene, YOLOv5s accurately identifies the bus and correctly predicts its submersion status, similar to YOLOv8s; however, the confidence level of YOLOv5s, even after data augmentation, shows limited improvement. YOLOv8s, on the other hand, demonstrates higher detection confidence and accuracy following data augmentation. In the high-risk scene, characterized by blurred or partially degraded images, YOLOv5s performs notably well. YOLOv5s detects targets that YOLOv8s fails to recognize, likely due to its capacity for handling noisy data. This difference in performance under extreme conditions suggests that the network structure of YOLOv5s may enhance detection in low-quality images, offering insights for

https://doi.org/10.5194/egusphere-2024-4053
Preprint. Discussion started: 10 March 2025

potential optimizations in YOLOv8s.

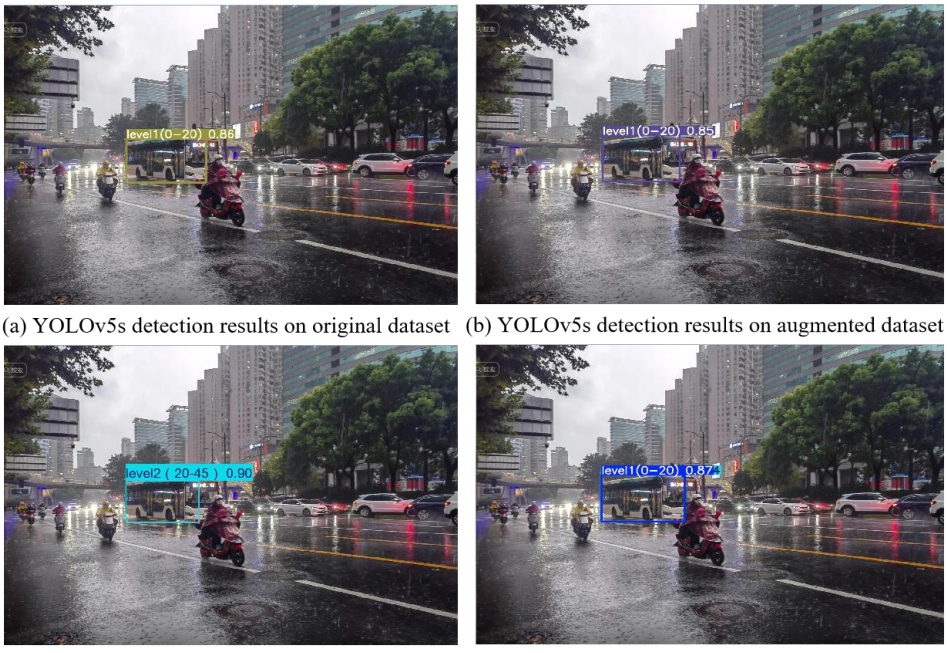

(a) YOLOv5s detection results on original dataset (b) YOLOv5s detection results on augmented dataset

(c) YOLOv8s detection results on original dataset (d) YOLOv8s detection results on augmented dataset

Fig. 14. Comparison of YOLO detection results in low flood risk scene with multiple vehicles present: (a) YOLOv5s detection results on original dataset; (b) YOLOv5s detection results on augmented dataset; (c) YOLOv8s detection results on original dataset; (d) YOLOv8s detection results on augmented dataset.

https://doi.org/10.5194/egusphere-2024-4053
Preprint. Discussion started: 10 March 2025

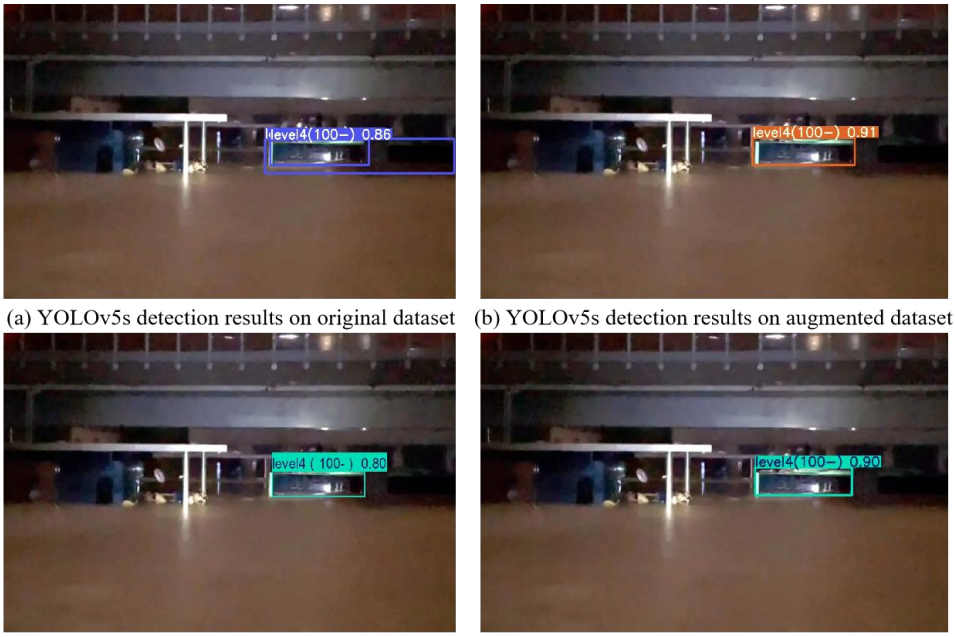

(a) YOLOv5s detection results on original dataset (b) YOLOv5s detection results on augmented dataset

(c) YOLOv8s detection results on original dataset (d) YOLOv8s detection results on augmented dataset

Fig. 15. Comparison of YOLO detection results in high flood risk scene with blurring and corruption: (a) YOLOv5s detection results on original dataset; (b) YOLOv5s detection results on augmented dataset; (c) YOLOv8s detection results on original dataset; (d) YOLOv8s detection results on augmented dataset.

4. Discussion

4.1 Impact of data augmentation

The dataset size plays a critical role in determining the performance of YOLOv8 models. The object detection experiment results in Section 3.1 demonstrate the positive effect of data augmentation on model performance. Models trained with the augmented dataset achieved substantial improvements, with mAP50 and mAP50-95 on the validation set increasing by over 10% and 20%, across all YOLOv8 configurations. This indicates that data augmentation significantly enhances detection accuracy while improving model stability and generalization across various IoU thresholds.

The impact of data augmentation on performance varies across different YOLOv8 models. YOLOv8n, the configuration with the fewest parameters, demonstrates the largest performance gain post-augmentation, with the most substantial increases in both mAP50 and mAP50-95. In contrast, YOLOv8s, which performed well on the original dataset, exhibits the smallest performance improvement after augmentation. This suggests that YOLOv8s is already highly effective at extracting key features of detection targets, even with a relatively small dataset. Although the performance gain for YOLOv8s is minimal, it consistently delivers

https://doi.org/10.5194/egusphere-2024-4053
Preprint. Discussion started: 10 March 2025

the best results across multiple experiments.

The data augmentation strategy significantly enhanced model performance in complex scene experiments. Prior to augmentation, all four YOLOv8 models may exhibited false detections and low confidence levels under challenging conditions such as low light at night, blurred imagery, and partial occlusions. Post-augmentation, however, each YOLOv8 model showed notable improvements in detection accuracy and confidence in complex scenes. For instance, in multi-vehicle environments, the augmented YOLOv8 models were able to accurately detect the submersion status of buses with high confidence, whereas pre-augmentation models failed to make correct identifications. These findings indicate that data augmentation plays a crucial role in enhancing model recognition capabilities under complex conditions, enabling more robust performance in the variable environments encountered in practical applications.

The enhancement in model performance achieved through the data augmentation strategy stems from the YOLOv8 model's robust learning and generalization capabilities. By increasing data diversity through augmentation techniques such as rotation, flipping, and random cropping, the model is compelled to extract the critical features of detection targets with greater precision. Additionally, the expanded dataset after augmentation provides a larger volume of annotated instances, enriching the training samples from which the model can learn. This enhanced dataset supports more robust feature extraction, contributing to overall performance gains.

4.2 Impact of detection target

In previous studies, cars have commonly been used for flood detection (Puliti and Astrup, 2022; Redmon et al., 2016; Wan et al., 2024; Zhong et al., 2024) . However, the diversity in car models limits annotation standardization and reduces the model’s generalization capability. Additionally, the relatively low height of cars constrains their effectiveness as reliable flood detection references. For instance, in Wan et al.’s study on complex scenes (Wan et al., 2024) , only sedans were successfully identified, while pickup trucks in the images were challenging to detect. In contrast, buses offer standardized body structures, greater urban coverage, and consistent height characteristics, making them a more promising reference object for flood detection. The experiments and validations in this study demonstrate the strong performance of the object detection model trained on bus images, with its PR curve closely approaching the upper-right corner. The best model achieved an mAP50 of 0.734 across all categories on the test dataset, surpassing the previous

https://doi.org/10.5194/egusphere-2024-4053
Preprint. Discussion started: 10 March 2025

study result of mAP50 at 0.707 (Wan et al., 2024). Moreover, since buses predominantly operate in busy or critical areas, their ability to withstand water directly impacts the stability of urban public transportation systems. The bus submersion-based detection approach developed in this study effectively enhances flood risk assessment accuracy, providing a more scientific basis for future urban flood monitoring and emergency management.

4.3 Recommended configurations for YOLOv8

Based on the comprehensive performance of different YOLOv8 configurations during training and in complex scenes, this study recommends prioritizing the YOLOv8s model for urban flood detection using bus imagery. Although the YOLOv8l model theoretically offers higher network complexity and parameter count, which should enable more granular feature extraction, its performance improvements in this experiment were not significant. In contrast, the YOLOv8s model demonstrated superior results across multiple performance metrics and achieved an effective balance between model accuracy, training time, and computational resource requirements. Therefore, in environments with limited resources and high computational costs, YOLOv8s has proven to be the most advantageous choice.

When computational resources and dataset availability are ample, YOLOv8m or YOLOv8l should be considered as priority options. As dataset size expands and more computational resources become available, the performance potential of YOLOv8m and YOLOv8l models may be more fully realized. With larger datasets, the deeper network structures and advanced feature extraction capabilities of YOLOv8m and YOLOv8l can better capture critical features and details of the targets, resulting in higher accuracy and stability in object detection.

5. Conclusions

This study proposes an urban flood detection method based on the YOLOv8 deep learning model, which accurately assesses flood risk levels by identifying the submersion state of buses. A dataset of 1,008 images depicting submerged buses was collected from online platforms and expanded to 2,184 images using data augmentation strategies. Subsequently, the submersion states of buses were annotated into four levels for training the object detection model. Finally, the performance of various YOLOv8 models was compared through data augmentation and complex scene validation experiments, resulting in the following experimental insights:

https://doi.org/10.5194/egusphere-2024-4053
Preprint. Discussion started: 10 March 2025

1) The highest detection accuracy for flood risk levels is achieved by YOLOv8s. Although YOLOv8m and YOLOv8l demonstrated comparable overall performance, they required significantly greater computational resources and training time.
2) The application of data augmentation significantly enhanced the detection accuracy and robustness of the YOLOv8 models, improving their recognition precision and generalization capabilities when confronted with complex scenes.
3) The use of buses as reference objects for flood detection presents notable advantages, including high consistency and standardized structure, overcoming the limitations of previous reference objects such as cars, thereby making them more suitable for urban flood detection.
4) This study offers configuration recommendations for YOLOv8 models tailored to urban flood detection based on the submersion state of buses.

This study supplements and extends existing research on flood detection by validating the feasibility and effectiveness of using buses as reference objects for the identification of urban flood risk levels. This study explores the application potential of bus submersion state detection within the YOLOv8 framework. This approach broadens the technical pathways for urban flood monitoring and provides crucial support for flood emergency management within urban transportation systems, demonstrating practical value in the field of disaster prevention and mitigation.

This study primarily relies on social media image recognition to determine flood risk levels. However, the model's performance remains limited in certain complex scenes, such as those involving extreme lighting conditions. Additionally, the model currently lacks the capability to quantitatively measure flood depth, which is critical for precise flood risk assessment. Future research will concentrate on devising methods for quantitative flood depth estimation using bus submersion states and creating noise-resistant model architectures to improve the model's applicability and precision.

Data availability:

Data will be made available on request.

Declaration of competing interest

The authors declare that they have no known competing financial interests or personal relationships that could have appeared to influence the work reported in this paper.

https://doi.org/10.5194/egusphere-2024-4053
Preprint. Discussion started: 10 March 2025

Computer Code Availability:

The code in this study can be obtained from the Git repository:

https://github.com/ydkyly/dataset_and_result.git.

Authorship Statement

Yanbin Qiu: Writing – original draft, Validation, Software, Methodology, Investigation. **Xudong Zhou:** Writing – review & editing, Validation. **Jiaquan Wan:** Writing – review & editing, Project administration, Validation. **Tao Yang:** Writing – review & editing, Supervision. **Lvfei Zhang:** Formal analysis, Validation. **Yuanzhuo Zhong:** Data curation, Validation. **Leqi Shen:** Data curation, Validation. **Xinwu Ji:** Validation.

https://doi.org/10.5194/egusphere-2024-4053
Preprint. Discussion started: 10 March 2025

References

Alizadeh Kharazi, B. and Behzadan, A. H.: Flood depth mapping in street photos with image processing and deep neural networks, Comput. Environ. Urban Syst., 88, 101628, https://doi.org/10.1016/j.compenvurbsys.2021.101628, 2021.

Baranowski, D. B., Flatau, M. K., Flatau, P. J., Karnawati, D., Barabasz, K., Labuz, M., Latos, B., Schmidt, J. M., Paski, J. A. I., and Marzuki: Social-media and newspaper reports reveal large-scale meteorological drivers of floods on Sumatra, Nat. Commun., 11, 2503, https://doi.org/10.1038/s41467-020-16171-2, 2020.

Bhola, P. K., Nair, B. B., Leandro, J., Rao, S. N., and Disse, M.: Flood inundation forecasts using validation data generated with the assistance of computer vision, J. Hydroinformatics, 21, 240–256, https://doi.org/10.2166/hydro.2018.044, 2018.

Chaudhary, P., D'Aronco, S., Leitão, J. P., Schindler, K., and Wegner, J. D.: Water level prediction from social media images with a multi-task ranking approach, ISPRS J. Photogramm. Remote Sens., 167, 252–262, https://doi.org/10.1016/j.isprsjprs.2020.07.003, 2020.

DeVries, B.: Rapid and robust monitoring of flood events using Sentinel-1 and Landsat data on the Google Earth Engine, Remote Sens. Environ., 2020.

Fohringer, J., Dransch, D., Kreibich, H., and Schröter, K.: Social media as an information source for rapid flood inundation mapping, Nat. Hazards Earth Syst. Sci., 15, 2725–2738, https://doi.org/10.5194/nhess-15-2725-2015, 2015.

Guan, Y., Zheng, F., Zhang, P., and Qin, C.: Spatial and temporal changes of meteorological disasters in China during 1950–2013, Nat. Hazards, 75, 2607–2623, https://doi.org/10.1007/s11069-014-1446-3, 2015.

Huang, J., Kang, J., Wang, H., Wang, Z., and Qiu, T.: A Novel Approach to Measuring Urban Waterlogging Depth from Images Based on Mask Region-Based Convolutional Neural Network, Sustainability, 12, 2149, https://doi.org/10.3390/su12052149, 2020.

Iqbal, U., Perez, P., Li, W., and Barthelemy, J.: How computer vision can facilitate flood management: A systematic review, Int. J. Disaster Risk Reduct., 53, 102030, https://doi.org/10.1016/j.ijdrr.2020.102030, 2021.

Jafari, N. H., Li, X., Chen, Q., Le, C.-Y., Betzer, L. P., and Liang, Y.: Real-time water level monitoring using live cameras and computer vision techniques, Comput. Geosci., 147, 104642, https://doi.org/10.1016/j.cageo.2020.104642, 2021.

Jiang, J., Liu, J., Cheng, C., Huang, J., and Xue, A.: Automatic Estimation of Urban Waterlogging Depths from Video Images Based on Ubiquitous Reference Objects, Remote Sens., 11, 587, https://doi.org/10.3390/rs11050587, 2019.

Jiang, J., Qin, C.-Z., Yu, J., Cheng, C., Liu, J., and Huang, J.: Obtaining Urban Waterlogging Depths from Video Images Using Synthetic Image Data, Remote Sens., 12, 1014, https://doi.org/10.3390/rs12061014, 2020.

Kankanamge, N., Yigitcanlar, T., Goonetilleke, A., and Kamruzzaman, Md.: Determining disaster severity through social media analysis: Testing the methodology with South East Queensland Flood tweets, Int. J. Disaster Risk Reduct., 42, 101360, https://doi.org/10.1016/j.ijdrr.2019.101360, 2020.

Li, J., Cai, R., Tan, Y., Zhou, H., Sadick, A.-M., Shou, W., and Wang, X.: Automatic detection of actual water depth of urban floods from social media images, Measurement, 216, 112891, https://doi.org/10.1016/j.measurement.2023.112891, 2023.

Liang, J.: A local thresholding approach to flood water delineation using Sentinel-1 SAR imagery, ISPRS J. Photogramm. Remote Sens., 2020.

https://doi.org/10.5194/egusphere-2024-4053
Preprint. Discussion started: 10 March 2025

Park, S., Baek, F., Sohn, J., and Kim, H.: Computer Vision–Based Estimation of Flood Depth in Flooded-Vehicle Images, J. Comput. Civ. Eng., 35, 04020072, https://doi.org/10.1061/(ASCE)CP.1943-5487.0000956, 2021.

Paul, J. D., Buytaert, W., and Sah, N.: A Technical Evaluation of Lidar-Based Measurement of River Water Levels, Water Resour. Res., 56, e2019WR026810, https://doi.org/10.1029/2019WR026810, 2020.

Puliti, S. and Astrup, R.: Automatic detection of snow breakage at single tree level using YOLOv5 applied to UAV imagery, Int. J. Appl. Earth Obs. Geoinformation, 112, 102946, https://doi.org/10.1016/j.jag.2022.102946, 2022.

Qian, Y., Chakraborty, T. C., Li, J., Li, D., He, C., Sarangi, C., Chen, F., Yang, X., and Leung, L. R.: Urbanization Impact on Regional Climate and Extreme Weather: Current Understanding, Uncertainties, and Future Research Directions, Adv. Atmospheric Sci., 39, 819–860, https://doi.org/10.1007/s00376-021-1371-9, 2022.

Redmon, J., Divvala, S., Girshick, R., and Farhadi, A.: You Only Look Once: Unified, Real-Time Object Detection, in: 2016 IEEE Conference on Computer Vision and Pattern Recognition (CVPR), 2016 IEEE Conference on Computer Vision and Pattern Recognition (CVPR), Las Vegas, NV, USA, 779–788, https://doi.org/10.1109/CVPR.2016.91, 2016.

Rosser, J. F., Leibovici, D. G., and Jackson, M. J.: Rapid flood inundation mapping using social media, remote sensing and topographic data, Nat. Hazards, 87, 103–120, https://doi.org/10.1007/s11069-017-2755-0, 2017.

Smith, L., Liang, Q., James, P., and Lin, W.: Assessing the utility of social media as a data source for flood risk management using a real-time modelling framework, J. Flood Risk Manag., 10, 370–380, https://doi.org/10.1111/jfr3.12154, 2017.

Voulodimos, A., Doulamis, N., Doulamis, A., and Protopapadakis, E.: Deep Learning for Computer Vision: A Brief Review, Comput. Intell. Neurosci., 2018, 1–13, https://doi.org/10.1155/2018/7068349, 2018.

Wan, J., Qin, Y., Shen, Y., Yang, T., Yan, X., Zhang, S., Yang, G., Xue, F., and Wang, Q. J.: Automatic detection of urban flood level with YOLOv8 using flooded vehicle dataset, J. Hydrol., 639, 131625, https://doi.org/10.1016/j.jhydrol.2024.131625, 2024.

Yang, Z. and Wang, Q.: MINING METHOD OF TRAFFIC IMPACT AREAS OF RAINSTORM EVENT BASED ON SOCIAL MEDIA IN ZHENGZHOU CITY, Int. Arch. Photogramm. Remote Sens. Spat. Inf. Sci., XLVIII-3/W1-2022, 79–86, https://doi.org/10.5194/isprs-archives-XLVIII-3-W1-2022-79-2022, 2022.

Zhong, P., Liu, Y., Zheng, H., and Zhao, J.: Detection of Urban Flood Inundation from Traffic Images Using Deep Learning Methods, Water Resour. Manag., 38, 287–301, https://doi.org/10.1007/s11269-023-03669-9, 2024.